Journal of Zhejiang University-SCIENCE A (Applied Physics & Engineering) in press
www.jzus.zju.edu.cn; www.springer.com/journal/11582
E-mail: jzus_a@zju.edu.cn

Research Article

https://doi.org/10.1631/jzus.A2300507

Design and performance study on adaptive sealing of a dry cabin for maintenance of submarine pipeline

Jin GUO[1,3], Xinghui TAN[1], Hai ZHU[1], Jiawang CHEN[4], Shidi JIN[1], Yuanjie CHEN[2], Jie CHEN[2], Ruiduo YIN[2]✉

[1]*Institute of Ocean Engineering and Technology, Zhejiang University, Zhoushan 316021, China*
[2]*Zhejiang Institute of Metrology, Hangzhou 310018, China*
[3]*Hainan Institute, Zhejiang University, Sanya 572025, China*
[4]*Donghai Laboratory, Zhoushan 316021, China*

Abstract: The underwater dry maintenance method based on a dry cabin can achieve the same maintenance quality provided on land. The establishment of a reliable seal between the dry cabin and the pipe is a prerequisite for the formation of a dry environment. In this paper, an airbag is proposed as the means to seal the dry cabin. ABAQUS finite-element software was used to study the influence of the physical characteristics of the airbag on deformation characteristics and sealing performance. We also studied the adaptive sealing mechanism of the airbag under the time-varying gap condition. The simulation results show that the peak contact stress of the airbag is close to the gas pressure, so the hardness and thickness of the airbag have little effect on it. Under time-varying gap conditions, the required inflation pressure increases with the size of the gap. The simulated relationship between the gap and the inflation pressure can be referred to in order to guide the control of the air pressure of the airbag during actual operation. Finally, the similarity between the test results and simulation results demonstrates the accuracy of the simulation results.

Key words: Submarine pipeline; Underwater dry cabin; Silicone airbag; Sealing performance

1 Introduction

Submarine pipelines are the main components of offshore oil (gas) field development and production systems, and some submarine pipelines have been in service for more than 30 years (Animah and Shafiee, 2018). Compared with land pipeline, submarine pipeline is exposed to the harsh marine environment for a long time. Pipelines have great failure probability due to the multiple effects of metal corrosion (Yang et al., 2017), ocean-current erosion (Yang et al., 2017), natural disasters (Badida, Balasubramaniam, and Jayaprakash, 2019), and strikes from ships's anchors (Gucma and Zalewski, 2003).

The traditional repair methods for submarine pipelines are mainly sea-surface dry repair and underwater wet repair (Drumond et al., 2018; Li, Chen, and Zhu, 2016; Mao et al., 2015). Surface dry repair involves a high cost and heavy workload, and underwater wet repair results in poor welding quality. Therefore, the dry repair method based on a dry cabin has been proposed. Since the underwater dry inspection method is carried out in an air environment, it becomes possible to apply the same inspection process used on land on the seabed, thereby improving the same quality of inspection and repair. A subsea pipeline dry cabin is necessary to provide an underwater dry environment. The seawater inside the cabin is discharged to form a dry working environment, and the establishment of a reliable seal between the dry cabin and the pipe is a prerequisite for the formation

✉ Ruiduo YIN, 306964154@qq.com
Jin GUO, https://orcid.org/0000-0002-2726-5936
Xinghui TAN, https://orcid.org/0009-0004-4989-0590
Hai ZHU, https://orcid.org/0000-0002-4681-163X
Jiawang CHEN, https://orcid.org/0000-0002-6351-0062
Shidi JIN, https://orcid.org/0009-0008-6412-0438
Yuanjie CHEN, https://orcid.org/0009-0005-7276-6982
Jie CHEN, https://orcid.org/0009-0006-1413-9830
Ruiduo YIN, https://orcid.org/0009-0005-1512-2603

Received Oct. 7, 2023; Revision accepted Jan. 19, 2024; Crosschecked

of a dry environment. Existing underwater dry cabins are sealed mainly by compressing solid rubber strips. For example, the world's first underwater dry-welded cabin (UWH) is sealed by squeezing rubber through hydraulic doors (Fleury and Schofield, 1979; Gaudiano, 1975; Pratt, Priest, and Castaneda, 1997). In addition, some cabins rely on underwater frogmen to install steel plates to squeeze rubber for sealing, such as UHC (Berge et al., 2008; Vernon and Werner, 2009) and the Habitat designed and built by DCN Diving (Toups, Morrison, and Harper, 2021; Tronskar and Lee, 2016).

Meanwhile, inflatable airbags are a sealing method widely used in large-scale energy and infrastructure projects for the advantages of high filling degree, large deformation degree, and sealing on demand. Jiang (2012) used a combination method of theory and experiment to study the stability and air-tightness of fast-sealing airbags in tunnels. By comparing and analyzing the heat resistance, flame retardant, wear resistance, hardness, and air permeability of different kinds of rubber, they identified the ideal fluoro rubber material. In order to effectively contain catastrophic accidents, Ma et al. (2022) designed a way to rapidly seal disaster areas with inflatable capsules. The dynamic response characteristics of a small inflatable airbag under an explosion shock wave were studied. To build a device to quickly close a pipeline in the event of explosion propagation and/or chemical leakage, Eisenreich et al. (2007) built an airbag capable of withstanding a pressure of up to 10 bar. The modeling and shape analysis of the airbag in the pipeline were completed with CFD technology.

In order to improve the sealing performance of such an airbag, some studies have examined the parameters that affect it. Dong et al. (2021) used experimental and simulation methods to study the effects of airbag location, height, and thickness of oil- and gas-pipeline cleaning balls on multi-airbag sealing-disc bending angles and airbag expansion ratios. Chen et al. (2019) discussed and optimized the relationship between inflation rate and airbag parameters (volume and pressure) by using common coupling surface analysis in MSC.Dytran finite-element software. Given the current problems with the stability and air tightness of fast-sealing airbags, Jiang et al. (2012) completed optimal selection of an airbag by comparing and analyzing the heat resistance, flame retardance, wear resistance, hardness, and air permeability of different types of rubber. After studying the stress characteristics and failure mechanism of conventional airbags, Chen et al. (2023) put forward a method to improve the blocking ability of conventional airbags through reinforcement. They established a force-analysis model of reinforced airbags under external pressure, revealed the reinforcement mechanism, and obtained the calculation formula for critical external pressure.

In this study, we used ABAQUS finite-element software to study the effect of the physical characteristics of an airbag on its sealing performance. We also investigated the adaptive sealing mechanism under time-varying gap conditions. The specific work was as follows: (1) uniaxial tests were carried out to obtain the stress-strain constitutive model of a silica-gel airbag; (2) ABAQUS was used to analyze the sealing and force characteristics of sealing airbags with five kinds of cross-section shapes; (3) under the constant-gap working conditions, the influence of material hardness, wall thickness, and inflation pressure on the deformation, mechanical, and sealing characteristics of the airbag were studied; (4) the sealing characteristics of the selected airbag were studied under time-varying gap conditions, and the adaptive sealing mechanism of the airbag was evaluated; and (5) a full-scale airbag pressure test was carried out to verify the rationality of the simulation results.

2 Objects to be sealed: subsea pipeline-maintenance dry cabin

Fig. 1a shows the dry cabin developed by our team for subsea pipeline inspection and repair. As shown in Fig. 1b, the cabin consists of a top-half cabin and two bottom-quarter cabins. The quarter cabin is hinged and fixed on the half cabin, and the opening and closing of the cabin are realized under the action of a hydraulic cylinder. The working depth of the dry cabin is less than 40m. The working principle is to establish a seal between the dry cabin and

the pipeline after dry cabin is closed, and then the water in the dry cabin is pumped out and the cabin is filled with high-pressure gas to form a dry environment. As shown in Fig. 1c, the sealing of dry cabins can be divided into two stages. The first stage is sealing the plane section between the half and quarter cabins, marked in green in Fig. 1c. The second stage is sealing the arc section between the dry cabin and the pipeline, as marked in blue in Fig. 1c. The sealing of the arc section is accomplished with a combination of EPDM foam material and an inflatable airbag. When the pipe has a bend angle, the arc section of the dry cabin is not coaxial with the pipe (that is, the pipe appears eccentric), resulting in uneven compression of the seal strip in the arc section. In order to solve the problem of seal failure caused by the poor adaptive performance of Ethylene Propylene Diene Methylene (EPDM) foam material, we propose an adaptive seal between the dry cabin and the pipe. The sealing properties of EPDM foams have been discussed in detail in our previous articles (Guo et al., 2024). Therefore, this paper mainly discusses the sealing characteristics of airbags. The airbag is supplied with gas through an air-compressor unit on the deck. As there is no specific standard for the selection and design of airbag seals, it was necessary to study the factors that affect airbag seal performance.

The sealing of the dry cabin is mainly achieved through the use of EPDM sealing strips, which have good resistance to damage. Airbags are only used to compensate for some gaps. Therefore, damage to the airbags will not lead to accidents, only to leaks.

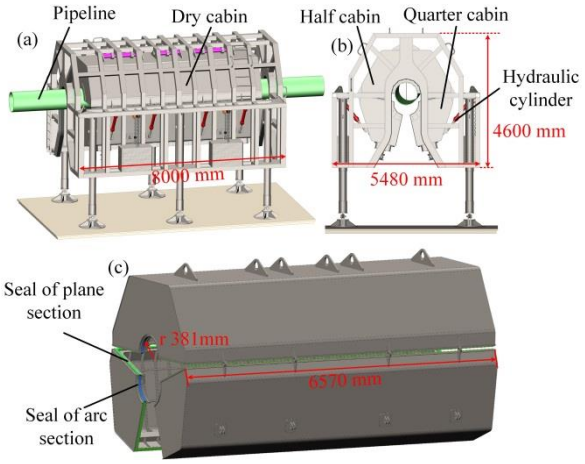

Fig. 1 (a) 3-D diagram of the dry cabin, (b) side view of the dry cabin, and (c) schematic diagram of the sealing type of the dry cabin

3 Methods

3.1 Silica-gel stress-strain constitutive model and seal-failure judgment criteria

The mechanical analysis of silica gel, a hyperelastic material, cannot be described only in terms of elastic modulus and Poisson's ratio like linear elasticity. Instead, the stress-strain data of silica gel airbags must be obtained by the uniaxial test, and the coefficient of the material constitutive model can be obtained by fitting the test data. One effective theory to describe the characteristics of hyperelastic materials is the constitutive theory based on the strain energy-density function.

In this study, we used the 2-parameter Mooney-Rivlin hyperelastic model for nonlinear finite-element analysis (Mooney, 1940; Rivlin, 1948; Rivlin and Saunders, 1951):

$$W = c_{10}(\bar{I}_1 - 3) + c_{01}(\bar{I}_2 - 3) + \frac{1}{d}(J-1)^2 \qquad (1)$$

where W is the strain energy potential, c_{10} and c_{01} are the material constants characterizing the material deflection, $\bar{I}_1$ and $\bar{I}_2$ are the first and second partial strain invariants, J is the determinant of the elastic deformation gradient, and d is the material incompressibility parameter. The expression is as follows:

$$d = (1-2\mu)/(c_{10} - c_{01}) \qquad (2)$$

where μ is Poisson's ratio.

From the relationship between Kirchoff stress tensor t_{ij} and Green strain tensor γ_{ij}:

$$t_{ij} = \frac{\partial \mathrm{W}}{\partial \bar{I}_1}\frac{\partial \bar{I}_1}{\partial \gamma_{ij}} + \frac{\partial \mathrm{W}}{\partial \bar{I}_2}\frac{\partial \bar{I}_2}{\partial \gamma_{ij}} + \frac{\partial \mathrm{W}}{\partial \bar{I}_3}\frac{\partial \bar{I}_3}{\partial \gamma_{ij}} \qquad (3)$$

The relationship between the principal stress σ_i of rubber material and its principal elongation ratio λ_i is as follows:

$$\sigma_i = 2\left(\lambda_i^2 \frac{\partial W}{\partial \bar{I}_1} + \frac{1}{\lambda_i^2}\frac{\partial W}{\partial \bar{I}_2}\right) + P \tag{4}$$

where P is hydrostatic pressure.

Three principal stress differences can be obtained from the above equation:

$$\begin{aligned}
\sigma_1 - \sigma_2 &= 2(\lambda_1^2 - \lambda_2^2)\left(\frac{\partial W}{\partial \bar{I}_1} + \lambda_3^2 \frac{\partial W}{\partial \bar{I}_2}\right) \\
\sigma_2 - \sigma_3 &= 2(\lambda_2^2 - \lambda_3^2)\left(\frac{\partial W}{\partial \bar{I}_1} + \lambda_1^2 \frac{\partial W}{\partial \bar{I}_2}\right) \\
\sigma_3 - \sigma_1 &= 2(\lambda_3^2 - \lambda_1^2)\left(\frac{\partial W}{\partial \bar{I}_1} + \lambda_2^2 \frac{\partial W}{\partial \bar{I}_2}\right)
\end{aligned} \tag{5}$$

For unidirectional tension or compression, $\sigma_2 = \sigma_3 = 0$, $\lambda_2^2 = \lambda_3^2 = 1/\lambda_1$, then

$$\sigma_1 = 2\left(\lambda_1^2 - \frac{1}{\lambda_1}\right)\left(\frac{\partial W}{\partial \bar{I}_1} + \frac{1}{\lambda_1}\frac{\partial W}{\partial \bar{I}_2}\right) \tag{6}$$

Based on equation (1), equation (7) can be obtained:

$$\frac{\partial W}{\partial \bar{I}_1} = C_{10}, \frac{\partial W}{\partial \bar{I}_2} = C_{01} \tag{7}$$

Substituting equation (7) into equation (6):

$$\frac{\sigma_1}{2\left(\lambda_1^2 - \frac{1}{\lambda_1}\right)} = C_{10} + \frac{1}{\lambda_1} C_{01} \tag{8}$$

The above equation is the basic formula for determining C_{10} and C_{01} by uniaxial tensile or compression test.

The criterion for seal failure is to compare the relationship between the maximum contact stress and the working stress. When the maximum contact stress is greater than the working pressure, it is considered that the seal has not failed.

3.2 Simulation model and mesh division

Since the distribution of the geometry and load characteristics of the arc section is the same in the circumference direction, we simplified the three-dimensional model to a two-dimensional model on a cross-section. In addition, for large dry cabins, the two-dimensional model can reduce the modeling workload and shorten simulation calculation time.

The Mooney-Rivlin hyperelastic model describing rubber elastic deformation was provided by ABAQUS finite-element software, which has been widely used in sealing research (Cui et al., 2014; Lan et al., 2019; Liu et al., 2022; Zhou, Chen, and Shi, 2015). Since the elastic modulus of steel is much larger than that of silica gel, the deformation of the dry cabin and pipe are negligible, so the dry cabin and pipe are set as rigid bodies. In the simulation model, the rigid body is defined as the primary face, and the sealed airbag is defined as the secondary face. Face-to-face contact pairs are established between airbags and rigid bodies. As shown in Fig. 2, in order to limit deformation of the airbag in the non-radial direction, the width of the groove of the cabin is designed to be the same width as the airbag. Since the bottom of the airbag is glued to the groove of the cabin body, the tangential contact behavior between the airbag and the bottom surface of the groove is set to non-slip. The tangential contact behavior between the airbag and the groove side wall, and between the airbag and the pipeline, is set as friction contact. The contact coefficient is 0.15. In addition, by specifying a starting point for full exposure to the fluid, as shown in Fig. 2, the pressure-penetration function in ABAQUS can simulate the phenomenon of fluid penetrating two contact surfaces (simulating the water pressure). The fluid pressure is loaded along the starting point to the contact surface on both sides, and the direction of pressure loading is perpendicular to the contact surface. When the contact stress (P_c) of a node is greater than the penetration pressure (P_p), loading is stopped.

Three analysis steps are used in the simulation. In the first step, the contact interference between the airbag and the dry cabin is solved. In the second step, air pressure (P_a) is applied to the inner wall of the airbag to simulate the inflation process of the airbag. In the third step, the fluid penetration function is applied to simulate the process of increasing the working pressure (P_p) on one side of the airbag.

As shown in Fig. 2, the airbags were suitably

sliced to divide the structured mesh. Mesh-convergence studies will also be discussed below.

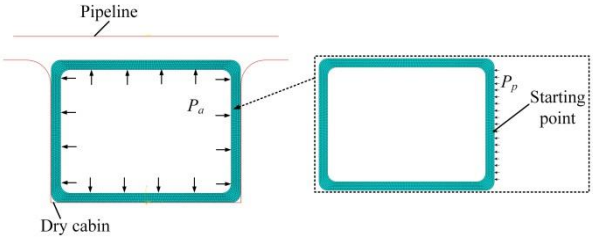

Fig. 2 Airbag meshing

For the uniaxial test, please refer to Section S1 of the electronic supplementary materials (ESM). For the airbag-expansion and seal-pressure test, please refer to Section S2 of the ESM.

4 Simulation cases

4.1 Airbags with different physical characteristics

4.1.1. Different section shapes

As shown in Fig. 3, the most widely used airbags on the market have five different cross-sectional shapes. Different cross-section shapes produce different deformation after inflation, making the bags suitable for sealing in different working conditions. In order to select the best airbag for sealing in the arc section between the dry cabin and the pipeline, the sealing performance of airbags with different section shapes will be studied. The detailed dimensions of the airbags are shown in Fig. S4. The wall thickness t_a and width w_a of the airbag studied are 1.5mm and 40mm, respectively. The gap g_a between the top of the airbag and the pipeline is 5mm. The airbag has a Shore hardness of 60HA and its stress-strain data is covered in the next section. In the simulation, the airbag inflation pressure P_a is 0.4MP, and the penetration pressure P_p is 0.2MPa.

Fig. 3a shows cross-section-1 (S1). This type of airbag has a large expansion stroke and good sealing performance, and is suitable for the application scenario that requires a large expansion amount.

Fig. 3b shows cross-section-2 (S2). This type of airbag is a modified version of S1, and is suitable for an ultra-high expansion ratio and working conditions with large sealing gaps. Due to its high ejection ratio and slightly poor pressure resistance, it is not suitable for high-pressure sealing conditions.

Fig. 3c shows cross-section-3 (S3). This type of airbag is mainly used for radial expansion sealing and can be used as a fixture. When expanding, the contact surface is wide, the sealing effect is good, and the sealing gap is small. It has excellent pressure resistance and is widely used in all kinds of sealing situations.

Fig. 3d shows cross-section-4 (S4), which is similar to S3. This type of airbag improves sealing performance against particles and dust with an optimized sealing-surface design, and is often used for sealing pharmaceutical and papermaking equipment. It also has good pressure resistance.

Fig. 3e shows cross-section-5 (S5). This type of airbag contains a base, which is easy to fix in place and does not shift or fall off easily, and offers large expansion, suitable for sealing conditions with large expansion requirements.

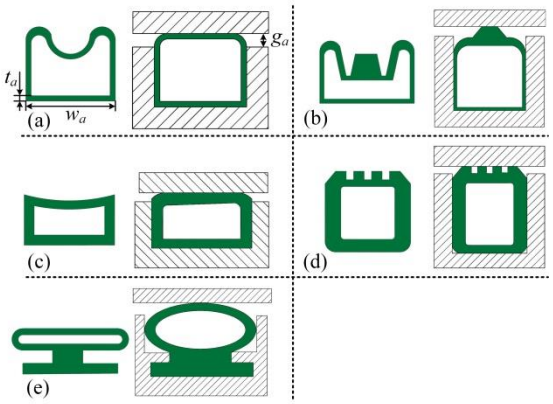

Fig. 3 Sealing airbags with different cross-sections, (a) section-1, (b) section-2, (c) section-3, (d) section-4, (e) section-5

4.1.2. Different hardness

Commercially available silicone airbags have Shore hardness between 50HA and 70HA. In order to accurately model the stress-strain constitutive model of the airbag in ABAQUS, we carried out uniaxial tensile and compression experiments on silica gel samples with Shore hardness of 50HA, 60HA, and 70HA. Each sample had 4 parallel samples. Fig. 4 shows the uniaxial test data for the samples. For each

curve, the area between the two dashed lines represents the distribution of the four test results. Under the same strain, the greater the hardness of the silica gel, the greater the stress, which is in line with the characteristics of the material.

According to the uniaxial test data, the specific methods to determine C_{10} and C_{01} in the Mooney-Rivlin constitutive model of airbags are as follows. σ_1 under different λ_1 is measured according to the test. $\frac{1}{\lambda_1}$ is taken as the horizontal coordinate and $\frac{\sigma_1}{2(\lambda_1^2-\frac{1}{\lambda_1})}$ is taken as the vertical coordinate. The test point is drawn in the coordinate system and fitted to a straight line. C_{10} is the intercept of this line, and C_{01} is the slope. Based on the fitting results, C_{10}, C_{01} and failure stress of silica gel with three hardness levels are shown in Table 1.

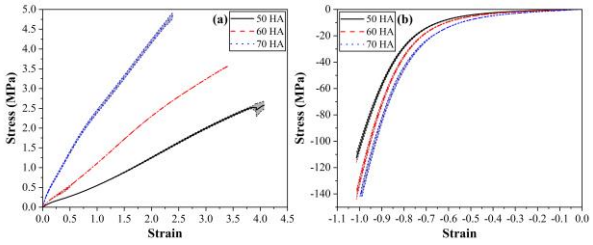

Fig. 4 Uniaxial test results for silica gel with different hardness, (a) uniaxial tensile, (b) uniaxial compression

Table 1 C_{10} and C_{01} of silica gel with three levels of hardness

Shore hardness	Failure stress (MPa)	C_{10}	C_{01}
50HA	2.55	0.299	-3.930× 10^{-3}
60HA	3.75	0.395	-5.217× 10^{-3}
70HA	4.77	0.412	-5.384× 10^{-3}

4.1.3. Different airbag wall thicknesses

The wall thickness t_a of the airbag also affects its sealing performance. Under the same inflation pressure, an airbag with thinner walls can produce greater deformation; that is, it can fill a larger gap. However, too-low wall thickness will reduce the strength of the airbag and the corresponding reduction of pressure resistance. Therefore, in order to select the appropriate wall thickness, it was necessary to study the deformation and stress characteristics of the airbag with different wall thicknesses. The wall thickness t_a of the airbag ranged from 1.5mm to 4mm.

4.2 Different sealing gaps g_a

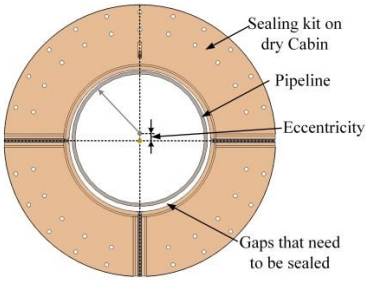

Fig. 5 Diagram of the eccentricity of the pipe relative to the dry cabin

As mentioned above, in the maintenance of a curved pipe, the dry cabin and pipe will have a different coaxial situation; that is, the pipe will be eccentric relative to the arc section of the dry cabin. The fact that the dry cabin sitting on sediment will also settle unevenly exacerbates this , as shown in Fig. 5. Section 4.1 discusses the influence of airbag physical characteristics on sealing performance at $g_a = 5$mm.

5 Results and Discussion

5.1 Mesh-convergence research

We studied mesh convergence using an airbag with a Shore hardness of 60HA and cross-section S3. The airbag width and height are 40mm and 30mm, respectively, and the thickness is 1.5mm. Based on the size of the airbag, we verified the functions of ABAQUS for simulating airbag inflation and pressure penetration. In the simulation, the airbag inflation pressure P_a is 0.4MP, and the penetration pressure P_p is 0.1MPa. Fig. 6 shows the shape of the airbag at three moments. As shown in Fig. 6b, the airbag expanded at a pressure of 0.4MPa. Under the constraint of the cabin, the airbag mainly expands in the vertical direction and fills the gap between the cabin body and the pipeline. The top of the airbag contacts the pipe and creates contact stress. As shown in Fig. 6c, $P_p = 0.1$MPa is applied to the right side of the airbag,

resulting in slight compression in the upper right corner of the expanded airbag.

Fig. 7 shows the change in the maximum contact stress and maximum Mises stress with the number of meshes. The specific values are shown in Table 2. Both stress measurements increases with the number of meshes. The change rate decreases as the number of meshes increases . When the mesh number increases from 2220 to 5394, the change rate of contact stress and Mises stress are both 0.08%. Compared with the smaller number of meshes, the change rate was significantly reduced. Therefore, we used a mesh with a size of 0.3mm in the following simulation model.

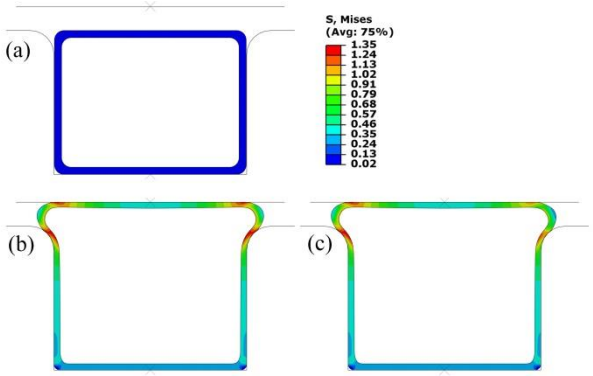

Fig. 6 Airbag Mises stress distribution at different moments, (a) at the initial moment, (b) applied gas pressure P_a, (c) applied penetration pressure P_p

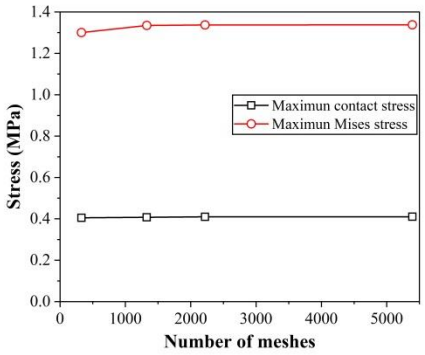

Fig. 7 Change in maximum contact stress and maximum Mises stress with the number of meshes.

Table 2 Maximum contact stress and maximum Mises stress correspond to different numbers of meshes

Mesh size (mm)	Mesh number	Maximum contact stress (MPa)	Rate of change	Maximum Mises stress (MPa)	Rate of change
0.8	328	0.404829	/	1.30044	/
0.4	1328	0.407413	0.64%	1.33502	2.66%
0.3	2220	0.409558	0.53%	1.33757	0.19%
0.2	5394	0.409891	0.08%	1.33767	0.08%

5.2 Influence of airbag characteristics on sealing performance

5.2.1 Influence of cross-section on sealing performance

In this section, the sealing characteristics of airbags with 5 kinds of section shapes are discussed. In the simulation, the P_a is 0.4MP, and the P_p is 0.2MPa. More detailed operating settings are described in Section 4.1. As shown in Fig. 3, the commonly used airbags on the market have five different cross-section shapes. Airbags with different cross-section shapes produce different deformation after aeration, that is, different sealing performance. As described above, we studied this in order to select the optimal airbag for sealing the arc section between the dry cabin and the pipeline.

Fig. 8a illustrates that the peak values of contact stress generated by airbags with different cross sections are significantly different. Due to the uneven contact surface at the top of the airbags with S2 and S4, large contact stress is generated, with similar stress magnitude. Because the top of the airbags with the other cross-sections is flat, the contact stress is

small. However, the contact stress of all airbags is greater than the penetration pressure of 0.2MPa, which meets the requirements of sealing. As shown in Fig. 8b, the uneven top surface of airbags with S2 and S4 result in stress concentration and large Mises stress. The Mises stress of airbag with S3 is small due to its regular shape and uniform inflation. Large Mises stress shortens airbag life. Failure of the conventional solid seal will only result in slow penetration of the liquid. However, destruction of the airbag will cause the seal to fail instantaneously, and the gap that was originally filled by the airbag will be immediately restored, causing a large influx of seawater into the dry cabin. Therefore, to ensure the safety of underwater operation of dry cabins, it is essential to keep Mises stress at a low level.

Thus, comprehensively considering the contact stress and Mises stress of the airbags with five types of cross-section, we selected airbag with S3 as the sealing tool for the dry cabin.

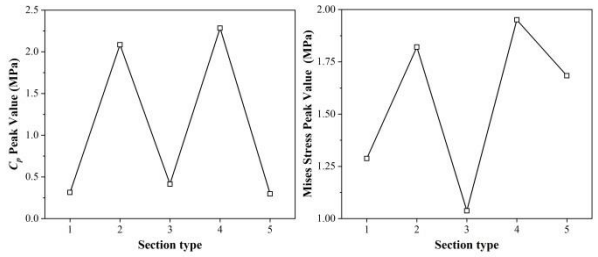

Fig. 8 (a) contact stress peak values of airbags with different cross-sections, and (b) Mises stress peak values of airbags with different cross-sections

5.2.2. Influence of airbag hardness on sealing performance

Cross-section-5 was selected as the final airbag type in the previous section. This section takes airbag-S3 as the research object and discusses the influence of hardness on airbag sealing characteristics. The material parameters of the airbags with three hardness levels were obtained by uniaxial testing and are discussed in detail in Section 4.1.2. In the simulation, the effect of water pressure was not considered ($P_p = 0$).

As shown in Fig. 9a, the peak contact stress of the airbag in the part in contact with the pipeline increases with inflation pressure, and the hardness has little effect on the peak contact stress. Since the sealing mechanism of the airbag is inflation and expansion, the peak contact stress is basically equal to the air pressure. As shown in Fig. 9b, as the deformation degree of the airbag increases with the air pressure, the Mises stress peak value also increases with the increase of inflation pressure. When the P_a is less than 0.5MPa, the Mises stress peak value of the hard airbag is larger. When the P_a is greater than 0.5MPa, the Mises stress peak of the airbag with hardness 50HA becomes the maximum. As shown in Fig. 10, the airbag with low hardness has a large deformation under relatively large P_a, and the part in contact with the chamfer of the cabin has large stretch, resulting in stress concentration. The larger the Mises stress, the more likely the material is to crack. In addition, large Mises stress will accelerate the stress relaxation of the rubber material, resulting in a decrease in "stiffness" and seal failure. Therefore, we ultimately selected the airbag with a hardness of 60HA.

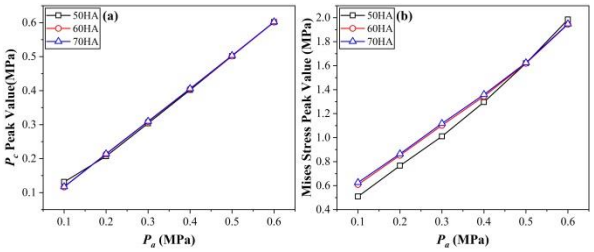

Fig. 9 The mechanical properties of airbags with three levels of hardness under different inflation pressures, (a) contact stress peak, (b) Mises stress peak

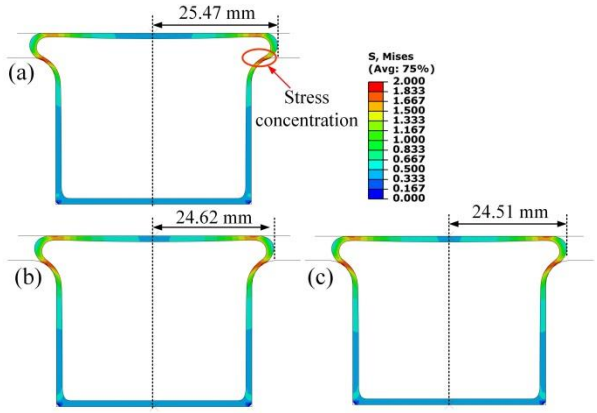

Fig. 10 Mises stress distribution at $P_a = 0.6$MPa of airbags with three levels of hardness, (a) 50HA, (b) 60HA, (c) 70HA

5.2.3. **Influence of airbag wall thickness on sealing performance**

In this section, we discuss the effect of wall thickness on the sealing characteristics of the airbag with a hardness of 60HA. The wall thicknesses t_a tested were 1mm, 1.5mm, 2mm, and 2.5mm. In the simulation, the effect of water pressure is not considered ($P_p = 0$).

As shown in Fig. 11a, consistent with the conclusion drawn above, the peak contact stress of the airbag increases with inflation pressure. Under the same air-pressure conditions, the contact stress generated by the thicker airbag is larger, but the difference is not particularly obvious. As shown in Fig. 11b, when the inflation pressure increases, the deformation degree of the airbag increases, and the Mises stress peak increases correspondingly. The larger the thickness of the airbag, the larger the cross-section area, and the smaller the stress under the same air pressure, so the smaller the deformation degree; that is, the smaller the Mises peak value. The Mises stress peak value showed a more obvious increasing trend with the increase of air pressure when the wall thickness of the airbag was small. The increasing trend tended to be gentle and gradually close with increasing airbag-wall thickness.

As shown in Fig. 12a, the maximum contact stress of the airbag is on both sides of the contact surface, which is different from the contact stress distribution of the O-ring (Huon et al., 2022; Wu and Li, 2022; Wu, Wang, and Wang, 2017). By comparing Fig. 12a and Fig. 13, it can be seen that locations with higher Mises stress values showed higher peak contact stress values. The larger the Mises stress, the greater the compression degree of the airbag, and thus the greater the contact stress between the airbag and the pipeline. The sealing surface width of an airbag with smaller wall thickness is larger because of its better ductility. With the increase of wall thickness, the width of the sealing surface decreases, but the peak value of contact stress on both sides increases, so the sealing performance increases with wall thickness. As shown in Fig. 13, with increasing wall thickness, the deformation degree of the airbag decreases continuously, and the overall Mises stress of the airbag shows a downward trend. With regard to contact stress and Mises stress, the performance of airbags with large wall thickness is better. However, Fig. 12b demonstrates that the large wall thickness results in poor ductility of the airbag, and the airbag not being able to expand to fill a larger gap. When the air pressure is 0.2MPa, the expansion height of the airbag with a wall thickness of 2.5mm is much less than 10mm, which is the maximum gap between the pipe and the cabin body. When the pressure at a working water depth of 0.4MPa is taken into consideration, the total pressure of 0.6MPa is close to the maximum working pressure of the air compressor. Therefore, an airbag with a wall thickness of 2.5mm is not conducive to filling the gap.

To ensure good gap-filling capacity and low Mises stress, we selected the airbag with a wall thickness of 2mm.

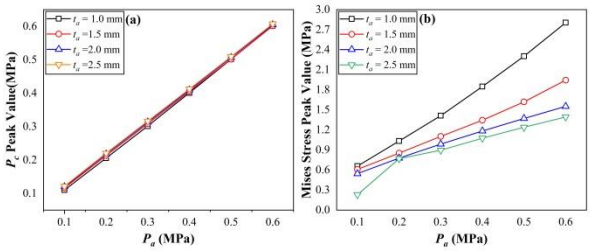

Fig. 11 Mechanical properties of airbags with four wall thicknesses under different inflation pressures, (a) contact stress peak, (b) Mises stress peak

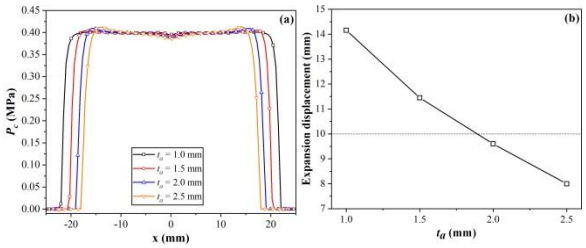

Fig. 12 (a) Contact stress distribution of airbags with four wall thicknesses, (b) the expansion displacement of airbags with four kinds of wall thickness in the y direction at $P_a = 0.2$MPa

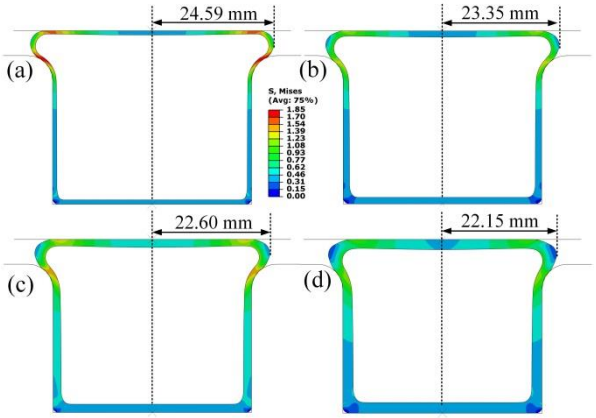

Fig. 13 Mises stress distribution of airbags with four wall thicknesses at $P_a = 0.4MPa$, (a) $t_a = 1$mm, (b) $t_a = 1.5$mm, (c) $t_a = 2$mm, (d) $t_a = 2.5$mm

5.3 Airbag sealing performance in different gaps

Because a curved pipe is eccentric relative to the arc section of the dry cabin, the distance (seal gap) between the top surface of the airbag and the pipe will be different in various circumferential positions. Therefore, it is necessary to clarify the relationship between the inflation pressure and different sealing gaps and study the sealing characteristics of the airbag under time-varying gap. Above, it was determined to use an airbag with a cross-section of S3, a hardness of 60HA, and a wall thickness of 2mm.

After the dry cabin sits at the bottom of 40m water depth, the ambient pressure of seawater is 0.4MPa, and the uninflated airbag is compressed. Therefore, it is necessary to fill the airbag with 0.4MPa of gas to restore it to its natural state. On the basis of 0.4MPa, a gasbag with larger gas pressure will expand and fill the gap between the pipe and the dry cabin. As shown in Fig. 14a, the required inflation pressure increases as the gap widens. The increasing trend tends to be flat with the widening of the gap. Inflation of the airbag by 5mm requires 0.533MPa, and 20mm requires 0.681MPa. The data in Fig. 14a can guide the control of airbag air pressure during the actual operation of a dry cabin. As shown in Fig. 14b, the Mises stress peak value increased along with airbag expansion, and the trend was similar to that of air pressure. However, the Mises stress of the airbag was less than 1MPa, which was far less than the failure stress of the uniaxial test (2.55MPa).

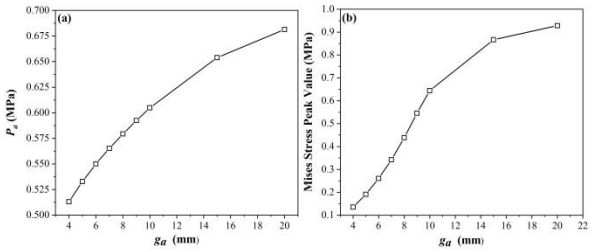

Fig. 14 (a) the air pressure required for the airbag to form a seal under different gap conditions, (b) the Mises stress peak value after the airbag formed a seal under different gap conditions

5.4 Airbag test

5.4.1. Airbag inflation height test

In order to verify the accuracy of the airbag elastic deformation constitutive model and the accuracy of simulating airbag inflation deformation using ABAQUS, we tested the expansion of customized airbags under different air pressures, as shown in Fig. 15a. Fig. 15b illustrates that the experimental results are consistent with the simulation results. When the air pressure is in the range of 0.015 MPa to 0.025 MPa, the experimental results are in agreement with the simulation results. When the air pressure is low or high, the error between the two is significant, with a maximum difference of 0.4mm. In summary, the test results verify the rationality of the simulation results.

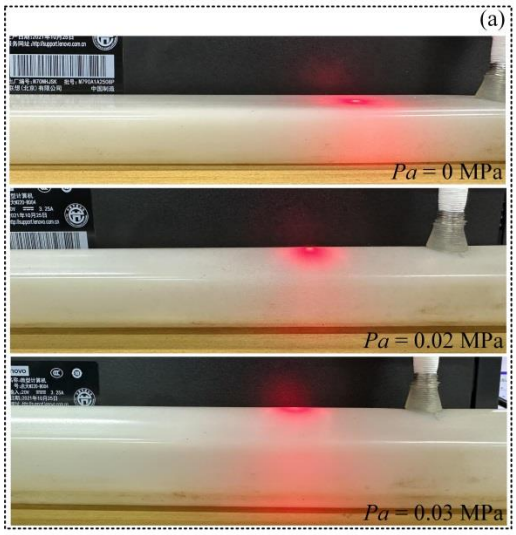

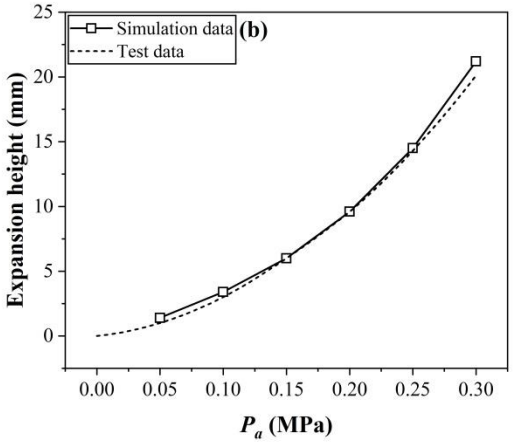

Fig. 15 (a) Diagram of airbag inflation, (b) relationship between airbag inflation height and air pressure

5.4.2. Airbag pressure-bearing capacity test

In order to verify the accuracy of the simulation results, we carried out a pressure test on the selected airbag. The inner diameter of the outer cylinder of the seal test cabin is 410mm, the outer diameter of the inner cylinder is 340mm, and the initial height of the airbag is 30mm (see fig. S3). Therefore, the gap to be filled by the airbag is 5mm, which is the same as the gap in the simulation. The width of the airbag is 40mm, the height is 30mm, the thickness is 2mm, the hardness is 60HA, and the diameter is 410mm (the same as the inner diameter of the outer cylinder).

To determine whether there was a leak in the test cabin, when the pressure increased to a certain level, pressurizing was stopped to observe whether there was a significant decrease in cabin pressure within half a minute. As shown in Fig. 16a, the test cabin was pressurized at a speed of 0.1MPa/s. During the test, the airbags were filled with gases of 0.1MPa, 0.2MPa, 0.3MPa, 0.4 MPa, and 0.5MPa in sequence. When the pressure in the test cabin was lower than that of the airbag, it increased continuously over time. When the cabin pressure was higher than that of the airbag, it dropped to a level equivalent to the airbag pressure after pressurization was stopped. After testing, the pressure-bearing capacity of the airbag under different inflation pressures was 0.118MPa, 0.211MPa, 0.308MPa, 0.401MPa, 0.5MPa, and 0.599MPa, corresponding to the gas levels given above.

Fig. 16b shows the simulation results of the peak contact stress generated by the airbag under different inflation pressures of 0.120MPa, 0.218MPa, 0.313MPa, 0.410MPa, 0.507MPa and 0.605MPa. The difference between these measurements and the test results was 1.5%, 3.0%, 1.7%, 2.1%, 1.3%, and 1.0%, respectively. The small difference may be caused by fabrication errors in the airbag. However, the test results can still explain the accuracy of the simulation calculation.

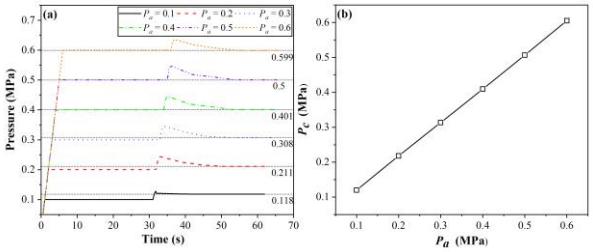

Fig. 16 (a) Pressure-bearing capacity test results of the airbag under different air pressures, (b) Simulation results of the peak contact stress generated by the airbag under different air pressures.

6 Conclusions

In this paper, we propose applying a non-standard airbag to seal a dry cabin for maintenance of submarine pipeline. We used ABAQUS finite-element software to study the influence of the physical characteristics of the airbag on its deformation characteristics and sealing performance. In addition, we studied the adaptive sealing mechanism of the airbag under the time-varying gap condition. Ultimately, a rectangular airbag with a hardness of 60HA and wall thickness of 2mm was selected after comprehensively considering airbag stiffness, gap-filling capacity, and Mises stress. The conclusions are as follows:

(1) Of five cross-section shapes, the rectangular cross-section resulted in the minimum Mises stress under the premise of satisfying the seal, which can improve the safety of airbag operation.

(2) The peak contact stress of the airbag is close to the level of the air pressure, so the hardness of the airbag has almost no effect on the peak contact stress. Airbag hardness had a slight effect on Mises stress.

(3) The contact stress generated by a thick airbag is greater, so sealing performance increases with wall

thickness. Greater wall thickness decreases the deformation degree, and the Mises stress shows a downward trend. However, high wall thickness results in poor ductility of the airbag, and an inability to expand to fill larger gaps.

(4) Under time-varying gap conditions, as the gap widens, the required gas pressure also increases. The Mises stress peak value increases with airbag expansion, and the trend is similar to that of gas pressure. The simulated relationship between the gap and the air pressure can guide air-pressure control of an airbag during actual operation of a dry cabin.

(5) The maximum difference between the the simulation results and those of the airbag expansion test is only 0.4mm, and the maximum difference between the pressure results of the airbag and the simulation results is only 3.0%, which indicates that ABAQUS can be used to accurately study the inflation deformation and sealing characteristics of airbags.

Acknowledgments

This work was supported by Eyas Program Incubation Project of Zhejiang Provincial Administration for Market Regulation (No. CY2023107); the PhD Scientific Research and Innovation Foundation of Sanya Yazhou Bay Science and Technology City (HSPHDSRF-2023-04-003); A Project Supported by Scientific Research Fund of Zhejiang Provincial Education Department (Y202353239); Zhoushan Field Scientific Observation and Research Station for Marine Geo-hazards, China Geological Survey (No. ZSORS-22-14).

Author contributions

Jin Guo designed the research. Xinghui Tan and Hai Zhu processed the corresponding data. Jin Guo and Shidi Jin wrote the first draft of the manuscript. Yuanjie Chen and Jie Chen helped to organize the manuscript. Jiawang Chen and Ruiduo Yin revised and edited the final version.

Conflict of interest

No potential conflict of interest was reported by the author(s).

References

Animah, Isaac, and Mahmood S, 2018. Condition Assessment, Remaining Useful Life Prediction and Life Extension Decision Making for Offshore Oil and Gas Assets. *Journal of Loss Prevention in the Process Industries*, 53:17–28. https://doi.org/10.1016/j.jlp.2017.04.030.

Badida, Pavanaditya, Yakesh B, et al., 2019. Risk Evaluation of Oil and Natural Gas Pipelines Due to Natural Hazards Using Fuzzy Fault Tree Analysis. *Journal of Natural Gas Science and Engineering*, 66(April):284–92. https://doi.org/10.1016/j.jngse.2019.04.010.

Berge, Mark, Lance B, et al., 2008. Underwater Habitat Clamp (UHC): An Innovative Partnership in Underwater Pipeline Repair. p 193–200 in *International Pipeline Conference*. Vol. 48609.

Chen J, Zheng YX, Zhong XK, et al., 2023. Working Mechanism and Testing of Emergency Reinforced Airbag Used for Blocking in Tunnels. *Tunnelling and Underground Space Technology*, 138:105201.

Chen, Yan, Chen GP, et al., 2019. Simulation of a Folded Airbag Inflating Underwater with IMM Method. P. 12004 in *IOP Conference Series: Materials Science and Engineering*. Vol. 531.

Cui, Kai B, Jun QQ, et al., 2014. Finite Element Analysis and Simulation of the Sealing Performance of Y-Ring Rubber Seal. *Applied Mechanics and Materials*, 444–445:1379–83. https://doi.org/10.4028/www.scientific.net/AMM.444-445.1379.

Dong JH, Liu SH, Hang Z, et al., 2021. Experiment and Simulation of a Controllable Multi-Airbag Sealing Disc of Pipeline Inspection Gauges (PIGs). *International Journal of Pressure Vessels and Piping*, 192:104422. https://doi.org/10.1016/j.ijpvp.2021.104422.

Drumond, Geovana P, Ilson P, et al., 2018. Pipelines, Risers and Umbilicals Failures: A Literature Review. *Ocean Engineering*, 148:412–25. https://doi.org/10.1016/j.oceaneng.2017.11.035.

Eisenreich N, Neutz J, Seiler F, et al., 2007. Airbag for the Closing of Pipelines on Explosions and Leakages. *Journal of Loss Prevention in the Process Industries*, 20(4):589–98. https://doi.org/10.1016/j.jlp.2007.04.030.

Fleury G, Schofield R, 1979. Dry Habitat Connections And Repairs Of Subsea Pipe-Line And Structures. in *Middle East Technical Conference and Exhibition*.

Gaudiano, Anthony V, 1975. A Summary of 26 Underwater Welding Habitat Jobs. in *Offshore Technology Conference*.

Gucma, Lucjan, Paweł Z, 2003. Damage Probability of Offshore Pipelines Due to Anchoring Ships. *Polish Maritime Research*, 10(4):6–12.

Guo J, Zhou QX, Tan XH, et al., 2024. Study on Sealing Performance and Optimization Design of a New Type Non-Standard Seal Strip of Submarine Pipeline Maintenance Dry Cabin. *Ocean Engineering*, 292:116508.

Huon, Carine, Avinash T, et al., 2022. Air, Helium and Water Leakage in Rubber O-Ring Seals with Application to Syringes. *Tribology Letters*, 70(2):35.

Jiang LM, Zhang YH, Huang ZA, et al., 2012. Experimental Study of Fast Sealing Airbag in Simulating Tunnel.

Procedia Engineering, 45:780–85. https://doi.org/10.1016/j.proeng.2012.08.239.

Lan WJ, Xin Z, Chen SS, 2019. Sealing Properties and Structure Optimization of Packer Rubber under High Pressure and High Temperature. *Petroleum Science*, 16(3):632–44. https://doi.org/10.1007/s12182-018-0296-0.

Li XH, Chen GM, Zhu HW, 2016. Quantitative Risk Analysis on Leakage Failure of Submarine Oil and Gas Pipelines Using Bayesian Network. *Process Safety and Environmental Protection*, 103:163–73. https://doi.org/10.1016/j.psep.2016.06.006.

Liu Y, Qian LQ, Zou JY, et al., 2022. Study on Failure Mechanism and Sealing Performance Optimization of Compression Packer. *Engineering Failure Analysis*, 136:106176. https://doi.org/10.1016/j.engfailanal.2022.106176.

Ma L, Liu SM, Wei GM, et al., 2022. Dynamic Response Characteristics of a Sealing Airbag under Different Impact Types and Impact Pressures. *ACS Omega*, 7(43):38589–99.

Mao DF, Chu G, Yang L, et al., 2015. Deepwater Pipeline Damage and Research on Countermeasure. *Aquatic Procedia*, 3:180–90. https://doi.org/10.1016/j.aqpro.2015.02.209.

Mooney M, 1940. A Theory of Large Elastic Deformation. *Journal of Applied Physics*, 11(9):582–92.

Pratt, Joseph A, Tyler P, et al., 1997. *Offshore Pioneers: Brown & Root and the History of Offshore Oil and Gas*. Elsevier.

Rivlin, Ronald S, 1948. Large Elastic Deformations of Isotropic Materials IV. Further Developments of the General Theory. *Philosophical Transactions of the Royal Society of London. Series A, Mathematical and Physical Sciences*, 241(835):379–97.

Rivlin, Ronald S, Saunders, 1951. Large Elastic Deformations of Isotropic Materials VII. Experiments on the Deformation of Rubber. *Philosophical Transactions of the Royal Society of London. Series A, Mathematical and Physical Sciences*, 243(865):251–88.

Toups, Earl L, Russell JM, et al., 2021. Development of a Micro-Habitat Hyperbaric Welding System. in *Abu Dhabi International Petroleum Exhibition & Conference*.

Tronskar, Jens P, Chon GL, 2016. Cofferdam and Hyperbaric "Live" Repair of Gas Pipeline Leaks. P. V004T03A004 in *International Conference on Offshore Mechanics and Arctic Engineering*. Vol. 49958. American Society of Mechanical Engineers.

Vernon, Tanya, Brandon W, 2009. Authentic Innovation: The Role of Apprenctice Learning in Engineering Education. p 439–47 in *ASME International Mechanical Engineering Congress and Exposition*. Vol. 43802.

Wu D, Wang SP, Wang XJ, 2017. A Novel Stress Distribution Analytical Model of O-Ring Seals under Different Properties of Materials. *Journal of Mechanical Science and Technology*, 31:289–96.

Wu JB, and Li L, 2022. Influence of Ambient Pressure on Sealing Performance of O-Ring in Deep-Sea Hydraulic System. *Ocean Engineering*, 245:110440.

Yang YS, Faisal K, Premkumar T, et al., 2017. Corrosion Induced Failure Analysis of Subsea Pipelines. *Reliability Engineering & System Safety*, 159:214–22.

Zhou SM, Chen P, Shi Y. 2015. Analysis on Sealing Performance for a New Type of Rubber Saddle-Shaped Sealing Ring Based on AQAQ S. *Procedia Engineering*, 130:1000–1009. https://doi.org/10.1016/j.proeng.2015.12.252.

Electronic supplementary materials

Sections S1 and S2

中文概要

题　目：用于维护海底管道的干舱自适应密封设计与性能研究

作　者：郭进[1,3]，谭星晖[1]，朱海[1]，陈家旺[4]，金诗迪[2]，陈元杰[2]，陈洁[2]，尹瑞多[2]

机　构：[1]浙江大学，海洋工程与技术研究所，中国舟山，316021；[2]浙江省计量科学研究院，中国杭州，310018；[3]浙江大学，海南研究院，中国三亚，572025；[4]东海实验室，中国舟山，316021；

目　的：以干式舱为基础的水下干式维护方法可以达到陆地上的维护质量。在干式舱和管道之间建立可靠的密封是形成干式环境的先决条件。本文旨在探讨气囊的物理特性对变形特性和密封性能的影响，研究气囊在时变间隙条件下的自适应密封机制。

创新点：1. 提出将非标准气囊应用于海底管道干舱的密封；2. 提出气囊在时变间隙条件下的自适应密封机制；

方　法：1. 进行单轴试验，得到硅胶气囊的应力-应变构成模型；2. 利用 ABAQUS 分析了五种截面形状的密封气囊的密封性和受力特性；3. 在间隙恒定的工作条件下，研究了材料硬度、壁厚和充气压力对气囊变形、力学和密封特性的影响；4. 研究了所选安全气囊在时变间隙下的密封特性，并讨论了安全气囊的自适应密封机理；5. 进行了全尺寸安全气囊压力试验，验证模拟结果的合理性。

结　论：1. 在满足密封的前提下，矩形截面安全气囊的 Mises 应力最小，可以提高安全气囊运行的安全性；2. 安全气囊的接触应力峰值与气压大小接近，因此安全气囊的硬度对接触应力峰值几乎没有影响。硬度对安全气囊的米塞斯应力有轻微影响；3. 厚气囊产生的接触应力更大，因此密封性能随着壁厚的增加而提高。随着壁厚的增加，气囊的变形程度减小，气囊的米塞斯应力呈下降趋势。但是，大的壁厚导致气囊的延展性较差，气囊膨

胀所能填充的间隙较小；4. 在间隙时变条件下，随着间隙的增大，所需的气体压力也随之增大。米塞斯应力峰值随气囊膨胀量的增加而增加，其趋势与气体压力的趋势相似。间隙与气压之间的模拟关系可以指导干式座舱实际运行时安全气囊气压的控制；5.气囊膨胀试验结果与模拟结果的最大差值仅为 0.4mm，气囊压力结果与模拟结果的最大差值仅为 3.0%，这表明利用 ABAQUS 可以准确研究气囊的充气变形和密封特性。

关键词：海底管道；水下干式舱；硅胶气囊；密封性能